Microbiota-dependent indole production stimulates the development of collagen-induced arthritis in mice

Brenda J. Seymour,[1] Brandon Trent,[1] Brendan E. Allen,[1] Adam J. Berlinberg,[1] Jimmy Tangchittsumran,[1] Widian K. Jubair,[1] Meagan E. Chriswell,[1] Sucai Liu,[1] Alfredo Ornelas,[2] Andrew Stahly,[1] Erica E. Alexeev,[2] Alexander S. Dowdell,[2] Sunny L. Sneed,[3] Sabrina Fechtner,[1] Jennifer M. Kofonow,[4] Charles E. Robertson,[4] Stephanie M. Dillon,[4] Cara C. Wilson,[4] Robert M. Anthony,[3] Daniel N. Frank,[4] Sean P. Colgan,[2] and Kristine A. Kuhn[1]

[1]Division of Rheumatology, Department of Medicine, and [2]Mucosal Inflammation Program and Division of Gastroenterology and Hepatology, Department of Medicine, University of Colorado Anschutz Medical Campus, Aurora, Colorado, USA. [3]Center for Immunology and Inflammatory Diseases, Division of Rheumatology, Allergy and Immunology, Department of Medicine, Massachusetts General Hospital, Harvard Medical School, Boston, Massachusetts, USA. [4]Division of Infectious Diseases, Department of Medicine, University of Colorado Anschutz Medical Campus, Aurora, Colorado, USA.

Altered tryptophan catabolism has been identified in inflammatory diseases like rheumatoid arthritis (RA) and spondyloarthritis (SpA), but the causal mechanisms linking tryptophan metabolites to disease are unknown. Using the collagen-induced arthritis (CIA) model, we identified alterations in tryptophan metabolism, and specifically indole, that correlated with disease. We demonstrated that both bacteria and dietary tryptophan were required for disease and that indole supplementation was sufficient to induce disease in their absence. When mice with CIA on a low-tryptophan diet were supplemented with indole, we observed significant increases in serum IL-6, TNF, and IL-1β; splenic RORγt$^+$CD4$^+$ T cells and ex vivo collagen-stimulated IL-17 production; and a pattern of anti-collagen antibody isotype switching and glycosylation that corresponded with increased complement fixation. IL-23 neutralization reduced disease severity in indole-induced CIA. Finally, exposure of human colonic lymphocytes to indole increased the expression of genes involved in IL-17 signaling and plasma cell activation. Altogether, we propose a mechanism by which intestinal dysbiosis during inflammatory arthritis results in altered tryptophan catabolism, leading to indole stimulation of arthritis development. Blockade of indole generation may present a unique therapeutic pathway for RA and SpA.

Introduction

Rheumatoid arthritis (RA) and spondyloarthritis (SpA) are 2 forms of inflammatory arthritis characterized by progressive joint inflammation leading to articular destruction. While there are genetic associations of MHC and non-MHC-risk alleles in both RA and SpA, these alone are not predictive of disease (1, 2). Environmental factors such as smoking have been associated with increased risk for RA and may provide an important trigger in genetically susceptible individuals (3). Identification of these specific environmental triggers, as well as the mechanisms by which they induce inflammation, may allow for prevention or early treatment of disease by removal of the trigger or specific blockade of the affected pathway.

Evidence of intestinal microbial dysbiosis in both RA (4–8) and SpA (9, 10), as well as substantial clinical overlap between SpA and bowel inflammation, suggests that specific microbes or microbial products may serve as an environmental trigger. In RA, this has led to the mucosal origins hypothesis that immune dysregulation in RA begins at mucosal sites (11–13). RA has a preclinical period of 5–10 years preceding clinically apparent disease characterized by intestinal dysbiosis, elevated inflammatory markers, circulating IgA plasmablasts, and autoantibody production at mucosal sites (11, 14), all of which point toward mucosal tissues as the origin of immune dysregulation. Recent identification of an arthritogenic strain of *Subdoligranulum* in individuals at risk for RA provides further evidence of a mucosal trigger (15). In SpA nearly 50% of patients have intestinal inflammation at the histologic level (16), and numerous studies support a gut/joint axis in SpA, in which immune dysregulation is initiated in the gut and then spreads systemically to the joint (17). Despite strong associative evidence of a mucosal origins hypothesis of RA and the gut/joint axis in SpA, the specific mechanisms by which microbes or microbial products trigger intestinal immune dysregulation in the context of inflammatory arthritis have not been elucidated.

We previously demonstrated a progressive gut dysbiosis in the murine model of collagen-induced arthritis (CIA) (18), in which autoimmune-prone DBA/1 strain mice are immunized with type II collagen (CII) emulsified in complete Freund's adjuvant (CFA) at days 0 and 21. In this model, dysbiosis is first observed between days 7–14, prior to the onset of clinically apparent disease, and progresses through day 35 (18), paralleling a microbiome-dependent increase in Th17 cytokines such as IL-17A, IL-22, and IL-23 (18, 19). Treatment with broad-spectrum antibiotics from days 21–35 resulted in markedly reduced CIA severity, suggesting a requirement for the microbiome in the development of disease (18).

Conflict of interest: The authors have declared that no conflict of interest exists.

Submitted: December 16, 2022; **Accepted:** December 13, 2023;
Published: December 19, 2023.
Reference information: *J Clin Invest*. 2024;134(4):e167671.
https://doi.org/10.1172/JCI167671.

Surprisingly, antibiotic treatment did not significantly reduce collagen-specific autoantibody production, but rather impaired complement activation by collagen-specific autoantibodies, which may have been due to altered antibody glycosylation. Together, these findings suggest a key role for the microbiome in shaping the immune response in CIA.

However, the mechanism or mechanisms by which the microbiome drive these inflammatory processes have not been identified. Observations of altered bacterial metabolomes have been described in both murine models of autoimmunity and in patients with autoimmunity (20–24), leading us to hypothesize that certain (yet unidentified) intestinal microbial metabolite(s) would play a key role in the development of CIA. We identified alterations in tryptophan (Trp) metabolism in CIA in a microbiome-dependent manner, with a substantial increase in indole (a bacterium-derived Trp metabolite) production in mice with CIA compared with unimmunized mice and antibiotic-protected CIA mice. We then tested whether indole supplementation was sufficient to induce CIA. We showed through 3 different methods that indole was indeed required for the development of CIA, and we characterized the cytokine, antibody, and cellular responses affected by indole treatment. Stimulation of human colon lamina propria mononuclear cells (LPMCs) with indole revealed upregulation of pathways similar to those observed in the mice, providing proof of concept that the observed effects of indole in CIA may be relevant to human disease. Altogether, our findings indicate that microbe-derived indole was required for the development of CIA through enhanced Th17 immunity and modulation of CII-reactive autoantibodies.

Results

Microbiome-dependent changes in Trp metabolism are associated with the development of CIA. We previously reported that bacterial dysbiosis and mucosal inflammation occurred prior to the onset of arthritis in the CIA model and that depletion of the microbiome through use of broad-spectrum antibiotics (ampicillin, vancomycin, metronidazole, and neomycin) resulted in an approximately 90% reduction in disease severity (18). To further query the effect of microbial dysbiosis on CIA, and because microbial metabolites can have profound effects on host immunity (25–27), we hypothesized that dysbiosis during CIA would alter the gut metabolome. Thus, we assessed a broad array of central energy and redox metabolites, yielding 244 named metabolites, by liquid chromatography with tandem mass spectrometry (LC-MS/MS) from the cecal contents of DBA/1 mice with CIA and compared them with untreated DBA/1 mice and mice treated with broad-spectrum antibiotics starting at CIA day 21 (CIA+Abx). Partial least-squares discriminant analysis (PLSDA) revealed a distinct microbiome-dependent metabolome in mice with CIA (Figure 1A). Volcano plot analysis identified several significant differences in Trp metabolites (5-hydroxyindoleacetate [5-HIAA], picolinic acid [PA], indoxyl, indolepyruvate [IPY], and L-Trp) in the CIA group compared with CIA+Abx, suggesting that CIA induced microbiome-dependent changes in Trp metabolism (Figure 1B).

Targeted HPLC quantification of 7 Trp metabolites from cecal contents revealed significant decreases in cecal Trp in the CIA group compared with CIA+Abx, along with a significant increase in indole (Figure 1, C and D), suggesting that microbiome-mediated Trp metabolism was skewed toward indole production in CIA. Decreased Trp in mice with CIA compared with CIA+Abx was consistent with microbial consumption of Trp, as reported previously (20). Trp is generally metabolized by 3 pathways: indole (primarily microbial), kynurenine, and serotonin (the latter 2 of which are primarily host pathways). To better assess which Trp pathways were affected in CIA, Trp metabolites that were identified in either the LC-MS/MS screen (Figure 1, A and B) or HPLC (Figure 1, C and D, and Supplemental Figure 1, A–D; supplemental material available online with this article; https://doi.org/10.1172/JCI167671DS1) were then manually mapped (Figure 1E) using the TrpNet.ca database (28) for reference, which provides pathway/relationship information on 108 Trp metabolites identified in the mouse and human microbiome. Of the metabolites screened in the indole pathway, 4 of 7 (indole-3-acetic acid [IAA], indole, indole-3-carboxaldehyde [I3A], and indoxyl) were significantly increased in CIA compared with CIA+Abx ($P < 5.9 \times 10^{5}$), 2 of 7 were increased but not statistically significantly (indolepropionic acid [IPA] and indole-3-acetaldehyde [IAAld]), and 1 of 7 was decreased (IPY). Of these metabolites, indole, I3A, IPA, and IPY are produced exclusively by the microbiome, whereas IAA, indoxyl, and IAAld can be produced by both the host and the microbiome (28). Although metabolites from the serotonin and kynurenine pathways were also significantly increased (5-HIAA [$P < 0.0001$], PA [$P = 0.0004$], and 2-aminomuconate [2-AM] [$P = 0.0008$]), we observed the largest differences within the indole pathway. Furthermore, 5HIAA and PA are produced exclusively by the host, not the microbiome (28). Because of the requirement for the microbiome in the development of CIA, we focused our attention on microbe-derived metabolites within the indole pathway, and in particular, indole, which had the highest differential abundance: a 528-fold increase in mice with CIA compared with the CIA+Abx group, and an 8-fold increase in mice with CIA compared with untreated DBA mice (Figure 1, D and E).

Because of the observed alterations in Trp metabolism in CIA, as well as our previous observations of altered Trp in SpA (9) and recent reports in murine lupus and experimental autoimmune encephalitis (EAE) models (20, 29), we queried whether Trp metabolism is altered in another murine model of inflammatory arthritis. We recently identified an arthritogenic bacterium, *Subdoligranulum didolesgii* isolate 7, that in mice stimulates spontaneous joint swelling, Th17 cell expansion, and production of autoantibodies in a pattern that mimics early RA (15). Using unbiased LC-MS/MS screening of metabolites from cecal contents of isolate 7–colonized mice, compared with nonarthritogenic *S. didolesgii* isolate 1–colonized mice, we observed a pattern of altered Trp metabolism similar to that seen in mice with CIA, with significant increases in IAA, indoxyl, and PA and decreases in IPY and L-tryptophan (Supplemental Figure 1E and asterisks in Figure 1E).

We then sought to identify the microbial source(s) of indole in CIA using paired 16S amplicon sequencing of fecal contents with cecal metabolomics by LC-MS/MS. Bacterial taxa belonging to the phyla Firmicutes (*Lactobacillales*, *Hydrogenoanaerobacterim*) and Bacteroidetes (*Barnesiella*, *Rikenellaceae*, *VC2.1-Bac22*) showed a strong Spearman's correlation with indoxyl levels (Supplemental

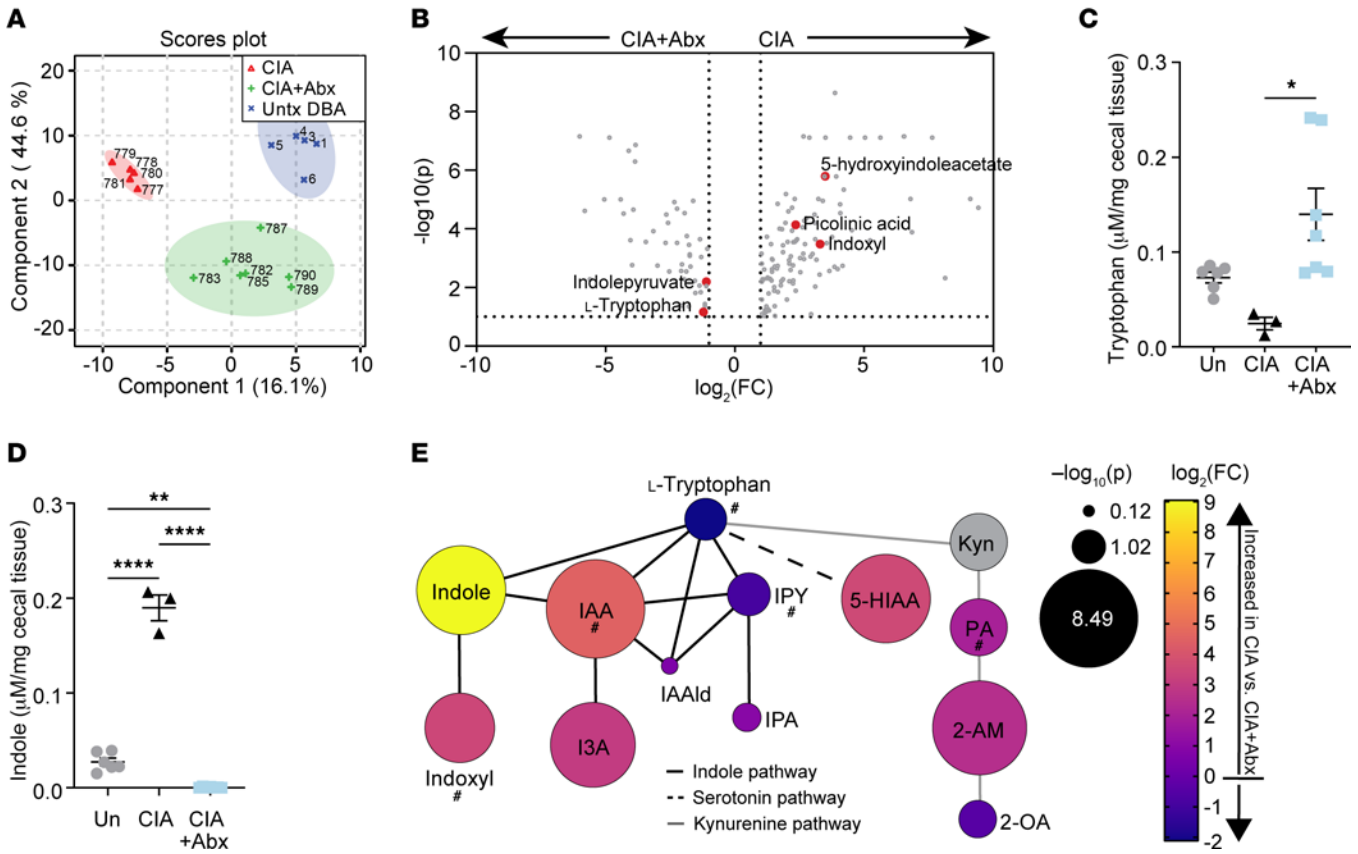

Figure 1. Intestinal metabolomics profiling identifies microbiome-mediated alterations in the tryptophan pathway in mice with CIA. CIA was induced in male 6-week-old DBA/1 mice, and cecal contents were harvested at day 35 from mice with CIA, mice with CIA that were depleted of microbiota by antibiotic administration after day 21, or untreated DBA/1 mice (Untx DBA). (**A** and **B**) LC-MS/MS was used to screen 244 metabolites from cecal contents of mice with CIA (n = 5), mice with CIA+Abx (n = 7), or untreated DBA/1 mice (n = 6). (**A**) PLSDA plot of CIA mice versus CIA+Abx mice versus untreated mice. (**B**) Volcano plot of CIA+Abx (left) versus CIA (right). (**C** and **D**) HPLC was used to quantify Trp pathway metabolites (indicated on the y axis) from cecal contents of mice with CIA (n = 3), mice with CIA+Abx (n = 7), or untreated DBA/1 mice (n = 6). All data are reported as individual mice (symbols) and the mean ± SEM (bars) after normalization to the weight (mg) of the cecal contents. *P < 0.05, **P < 0.01, and ****P < 0.0001, by 1-way ANOVA with Bonferroni's correction for multiple comparisons. (**E**) Graphical representation of Trp metabolism pathways showing Trp metabolites identified in the LC-MS/MS analysis (**A** and **B**) and HPLC analysis (**C** and **D**). The $\log_2$(fold change [FC]) was calculated for CIA versus CIA+Abx and is represented by a color gradient from yellow (greater increase in CIA) to blue (greater increase in CIA+Abx). The size of each circle represents the $-\log_{10}$(P value) of an unpaired Student's t test between CIA versus CIA+Abx. Kyn, kynurenine; 2-OA, 2-oxoadipate. The pound signs in **E** denote trends in metabolites that were also observed in *Isolate 7*-colonized mice. Lines denote pathways: black, indole; dashed line, serotonin; gray, kynurenine.

Figure 1F). Paired indole-16S data were not available, so indoxyl was used as a proxy in the Spearman's correlation (indole is metabolized by hepatic CYP450 enzymes into indoxyl, ref. 30). Of the taxa that correlated with indoxyl, all were elevated in CIA compared with CIA+Abx (Supplemental Figure 1G), indicating that their expansion may result in greater indole production. Finally, we found that indole levels significantly correlated with disease severity in mice with CIA (Supplemental Figure 1H). These results, in addition to observations of altered Trp metabolism in patients with SpA and RA (9, 31–35), prompted us to further interrogate the role of bacteria-derived Trp metabolites in inflammatory arthritis.

Bacterial Trp catabolism to generate indole is required for the development of inflammatory arthritis in CIA. Next, we hypothesized that dysbiosis following CIA induction leads to increased indole production, which then enhances disease severity. We first tested whether indole could reverse the disease protection afforded by antibiotic-induced ablation of microbiota during CIA (18). As done previously (18), we induced CIA by immunizing mice with bovine type II collagen in CFA on days 0 and 21. On day 21, antibiotics including ampicillin, metronidazole, neomycin, and vancomycin were added to the drinking water. In addition, 0.1 mg/mL indole was included in the drinking water for 1 group of mice at this time. We observed an approximately 3-fold increase in arthritis severity 35 days after the initial immunization when we added indole to the drinking water of CIA+Abx mice (Figure 2A), suggesting that indole was sufficient to at least partially replace the role of the bacterial microbiome during CIA.

We then tested the effects of various levels of dietary Trp on CIA. Because Trp is an essential amino acid, mice fed a Trp-deficient (0% Trp) diet lose approximately 15%–20% of their body weight within 7 days (20). Therefore, similar to previous studies (20), we replaced the Trp-deficient diet with a Trp-sufficient (TS) diet, which contains 0.18% L-Trp, on the weekends for a cumulative Trp-low (TL) diet (0.05% L-Trp). With this TL diet, we found that mice lost no more than 15% of their starting body weight (Supplemental Figure 2A). To ensure consistent dosing, indole (10

mM) or vehicle (0.33% methanol) was added back by oral gavage every other day starting on day 0 for the duration of the experiment. The TL+Vehicle group had a significant reduction in disease severity and incidence, with an average CIA score of approximately 1 (Figure 2B) and a CIA incidence of 55% (Supplemental Figure 2B), suggesting a requirement for dietary Trp in the development of CIA. Adding back indole resulted in a 4.5-fold increase in CIA severity compared with that seen in TL+Vehicle mice (Figure 2B), with a CIA incidence of 92% (Supplemental Figure 2B). We observed no significant difference in CIA scores or incidence in the TL+Indole group compared with the TS+Vehicle group, suggesting that indole supplementation fulfilled the requirement for dietary Trp in the development of CIA. Evaluation of pathology by H&E staining in a subset of mice revealed a significant decrease in inflammatory infiltrates, pannus, and bone resorption in the TL+Vehicle group compared with the TS+Vehicle group, which was restored with indole supplementation (Figure 2C and Supplemental Figure 2, C–G). Across all groups, the histologic inflammation score significantly correlated with the macroscopic arthritis score at day 35 (Supplemental Figure 2H).

Trp is an essential amino acid in mammals and can be synthesized from indole by microbial *Tryptophan synthase* (*TrpB*) (36) (Figure 2D). Thus, we investigated whether the reversal of TL-mediated protection in CIA with indole supplementation is due to the restoration of Trp levels by *TrpB*. HPLC analysis of cecal metabolites at CIA day 35 did not show a significant difference in Trp levels between TL+Vehicle and TL+Indole mice, and both groups had significantly lower cecal Trp levels than did TS+Vehicle mice (Figure 2E), suggesting that indole was not acting as a substrate for Trp synthesis. These data suggest that the differences in disease severity between TL+Vehicle and TL+Indole mice cannot be explained by Trp availability but rather is likely due to an effect of indole on either the host or the microbiome.

To further query the specific requirement for indole in CIA, we targeted microbial *Tryptophanase A* (*TnaA*), which is the sole enzyme responsible for indole production (37, 38) (Figure 2D). Germ-free DBA/1 mice were colonized with 10^8 CFU of either an *E. coli* K12 strain (BW25113 *ΔtnaA*), which is unable to produce indole due to deletion of *Tryptophanase A* (39), or an isogenic control (*E. coli* BW25113 *ΔbcsQ*), which produces normal levels of indole. Mice were maintained on standard rodent chow containing 0.2% L-Trp. Stable colonization of both *ΔtnaA* and *ΔbcsQ* was confirmed by quantitative PCR (qPCR) using global rpoB primers (Supplemental Figure 2I). Mice colonized with *ΔtnaA* had a significant, approximately 5-fold reduction in CIA severity compared with the *ΔbcsQ* control group (Figure 2F). HPLC analysis of cecal contents on day 35 confirmed that indole was only produced in the *ΔbcsQ* controls (Figure 2G). Together, these results suggest that indole produced by microbial *Tryptophanase A* was required for the development of CIA.

Indole minimally impacts bacterial dysbiosis due to a TL diet. We next sought to identify the mechanism through which indole incites disease. While we hypothesized that indole has a direct immunogenic effect on the host, leading to the development of CIA, an alternate hypothesis is that indole indirectly affected disease outcomes through its effects on the microbiome (40), as previous studies have shown that fecal transfer of "arthritogenic" or "nonarthritogenic" microbiomes predicts CIA severity and susceptibility in recipient mice (19). 16S rRNA gene sequencing of fecal contents revealed that α-diversity was lowest in the TS+Vehicle group (Figure 3, A–C). Interestingly, although the TL+Indole group developed levels of arthritis severity similar to those in the TS+Vehicle group, the TL+Indole group maintained higher α-diversity (Figure 3, A–C). β-Diversity was most significantly affected by the TL diet, as mice in the TS+Vehicle group showed greater dissimilarity from the TL+Vehicle and TL+Indole groups by principal component analysis (PCA) (Figure 3D and Supplemental Figure 3A) and permutational multivariate ANOVA (PERMANOVA) (Figure 3E and Supplemental Figure 3B). We then identified individual bacterial taxa driving the observed differences in microbial diversity. Ten taxa were expanded in the TS+Vehicle group compared with the TL+Vehicle group (FDR-corrected $P < 0.05$; Figure 3, F and G), including several that we have previously shown to be expanded in CIA (e.g., *Lachnospiraceae*) (18). Conversely, *Turicibacter*, *Clostridium*, and *Peptostreptococcaceae* were significantly elevated in the TL+Vehicle group compared with TS+Vehicle group (FDR-corrected $P < 0.05$; Figure 3, F and G). These 3 genera also accounted for the largest effect sizes in the comparison of the TS+Vehicle and TL+Indole groups (FDR-corrected $P < 0.05$; Figure 3, H and I). No taxa were found to be differentially abundant between the TL+Vehicle and TL+Indole groups ($n = 10$ per group) after adjusting P values for multiple comparisons (i.e., all FDR-corrected P values were greater than 0.05) (Supplemental Figure 3, C and D). Taken together, the microbiome-profiling results suggest that dietary tryptophan significantly affected fecal bacterial communities but that indole supplementation only minimally altered the diversity and composition of the fecal microbiota and probably does not explain the arthritis phenotype observed following indole supplementation.

Indole induces a unique inflammatory cytokine signature in CIA. Because the effects of indole on the fecal microbiota were minimal in the setting of a TL diet, we then assessed the effect of indole on immune cell function in CIA. First, because proinflammatory cytokines are key mediators of disease in CIA, RA, and SpA, we assessed the effects of the TL diet and indole supplementation on serum cytokine production throughout the course of CIA. Terminal serum was collected from mice with CIA at days 14 and 21 and at the plateau of disease severity (days 35–50, depending on the experiment). To account for experiment-to-experiment variability, serum cytokine concentrations were normalized to the mean of the TS+Vehicle group for each experiment and time point to allow for better group-to-group comparisons at each time point. Cytokine concentrations of the TS+Vehicle group (which were used for normalization) are shown in Supplemental Figure 4, A–F, compared with naive (unimmunized) DBA/1 mice.

There were no significant differences between groups in any of the cytokines measured at CIA days 14 and 21 (prior to arthritis onset). However, by the plateau of disease (CIA days 35–50), the TL+Vehicle diet resulted in a significant reduction in IL-6, a trend toward decreased IL-1β, and a significant increase in IL-10 compared with mice on the TS+Vehicle diet at CIA day 35+, but not at earlier time points (days 14 and 21) (Figure 4, A–C). These findings are consistent with the requirement for both IL-6 and IL-1β in the development of CIA and the protective role of IL-10 (41–43).

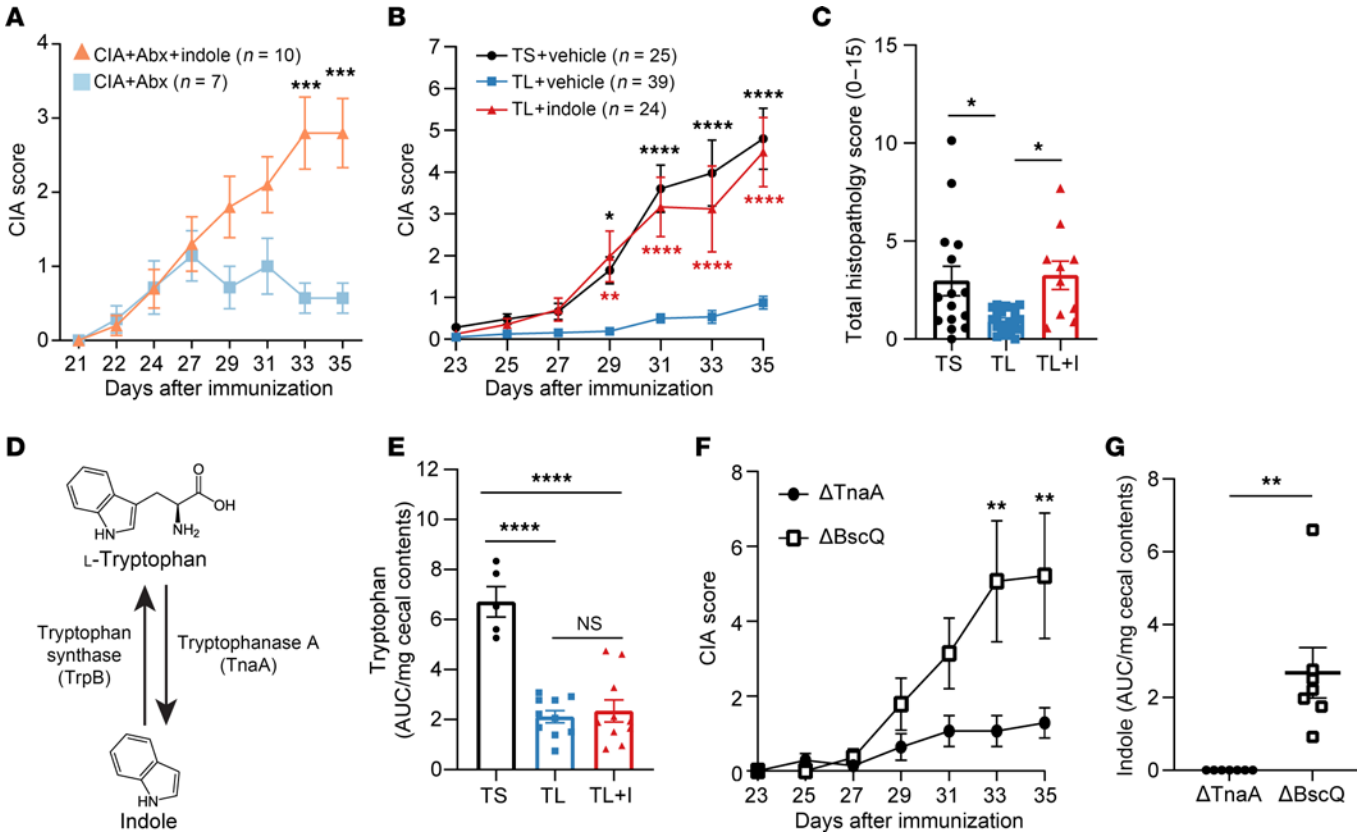

Figure 2. Indole is required for CIA. (**A**) CIA was induced in 6-week-old male DBA/1 mice. On days 21–35, mice were treated with antibiotics with or without 0.1 mg/mL indole in the drinking water, and arthritis scores were assessed every other day. $n = 10$ (Abx+Indole); $n = 7$ (CIA+Abx). (**B**) Six-week-old male DBA/1 mice were fed a TL or TS diet starting on day –1 and through the duration of the experiment. Following induction of CIA, mice were treated with indole (200 μL of a 10 mM solution) or vehicle control (0.33% methanol) by oral gavage every other day starting on day 0. Arthritis scores were assessed every other day from days 21–35. $n = 39$ (TL+Vehicle), $n = 24$ (TL+Indole), and $n = 25$ (TS+Vehicle), pooled from 5 independent experiments. Red asterisks: TL+Indole versus TL+Vehicle; black asterisks: TS+Vehicle versus TL+Vehicle. TS+Vehicle versus TL+Indole was not statistically significant. (**C**) The sum of the inflammation, pannus, and bone erosion score of H&E-stained paws is plotted as the total histology score (maximum score of 15). $n = 10$–20, pooled from 2 independent experiments. (**D**) Schematic of Trp breakdown into indole by bacterial *Tryptophanase A* and Trp synthesis from indole by bacterial *Tryptophan synthase*. (**E**) HPLC analysis of Trp in cecal contents from mice with CIA at day 35, plotted as the AUC, normalized to the weight (mg) of the cecal contents. $n = 5$–10, from 1 experiment. (**F**) Six-week-old male germ-free DBA/1 mice were colonized with *E. coli BW25113* mutants (*ΔtnaA* or *ΔBcsQ*) with 10^8 CFU by oral gavage on day –7 before CIA induction. $n = 7$ per group. (**G**) HPLC analysis of indole in cecal contents from CIA mice colonized with either *ΔtnaA* or *ΔBcsQ* at CIA day 35. Indole levels were plotted a the AUC per milligram of cecal content weight. Data are reported as the mean ± SEM. $^*P < 0.05$, $^{**}P < 0.01$, $^{***}P < 0.001$, and $^{****}P < 0.0001$, by 2-way ANOVA with Bonferroni's correction for multiple comparisons (**A**, **B**, and **F**), 1-way ANOVA with Bonferroni's correction for multiple comparisons (**C** and **E**), and unpaired 2-tailed Student's *t* test (**G**).

Indole supplementation significantly restored IL-1β and IL-6 levels at day 35+ (Figure 4, A and B). Surprisingly, despite nearly identical CIA severity in the TL+Indole and TS+Vehicle groups (Figure 2B), indole supplementation did not fully replicate the cytokine pattern observed in TS+Vehicle mice. Rather, we found that indole supplementation created a unique cytokine signature compared with that of the TS+Vehicle group, with significant increases in TNF and IFN-γ levels (Figure 4, D and E) and a small, but not significant, increase in IL-17A levels (Figure 4F, $P = 0.052$). IL-22, IL-23, and GM-CSF were also measured on day 35 but were either at or below the limit of detection (Supplemental Figure 4, G–I). Altogether, these data suggest that indole induced a unique proinflammatory signature in CIA.

Indole alters autoantibody pathogenicity. Another hallmark of CIA is the development of collagen-specific (CII-specific) autoantibodies (44, 45). As such, we queried whether indole affects the production of CII antibodies. We observed no significant differences in total IgG, anti–CII IgG, or germinal center B cell numbers between the groups (Supplemental Figure 5, A–C), and anti–CII IgG levels did not correlate with CIA severity (Supplemental Figure 5D), suggesting that the arthritis severity observed in the TL+Indole compared with the TL+Vehicle groups cannot be attributed solely to anti-CII autoantibody quantity, in agreement with previous studies (18, 46).

We then hypothesized that indole may affect the function, rather than quantity, of anti-CII antibodies. Indeed, we have previously demonstrated reduced complement fixation by anti-CII antibodies in CIA+Abx mice (18), suggesting that microbial stimuli may alter the ability of anti-CII antibodies to activate complement, thus altering their pathogenicity. In serum from TL+Indole mice compared with TL+Vehicle mouse serum, we observed an increase in complement fixation by anti-CII antibodies (Figure 5A). Complement deposition in the joints followed the same pattern, with a significant decrease in

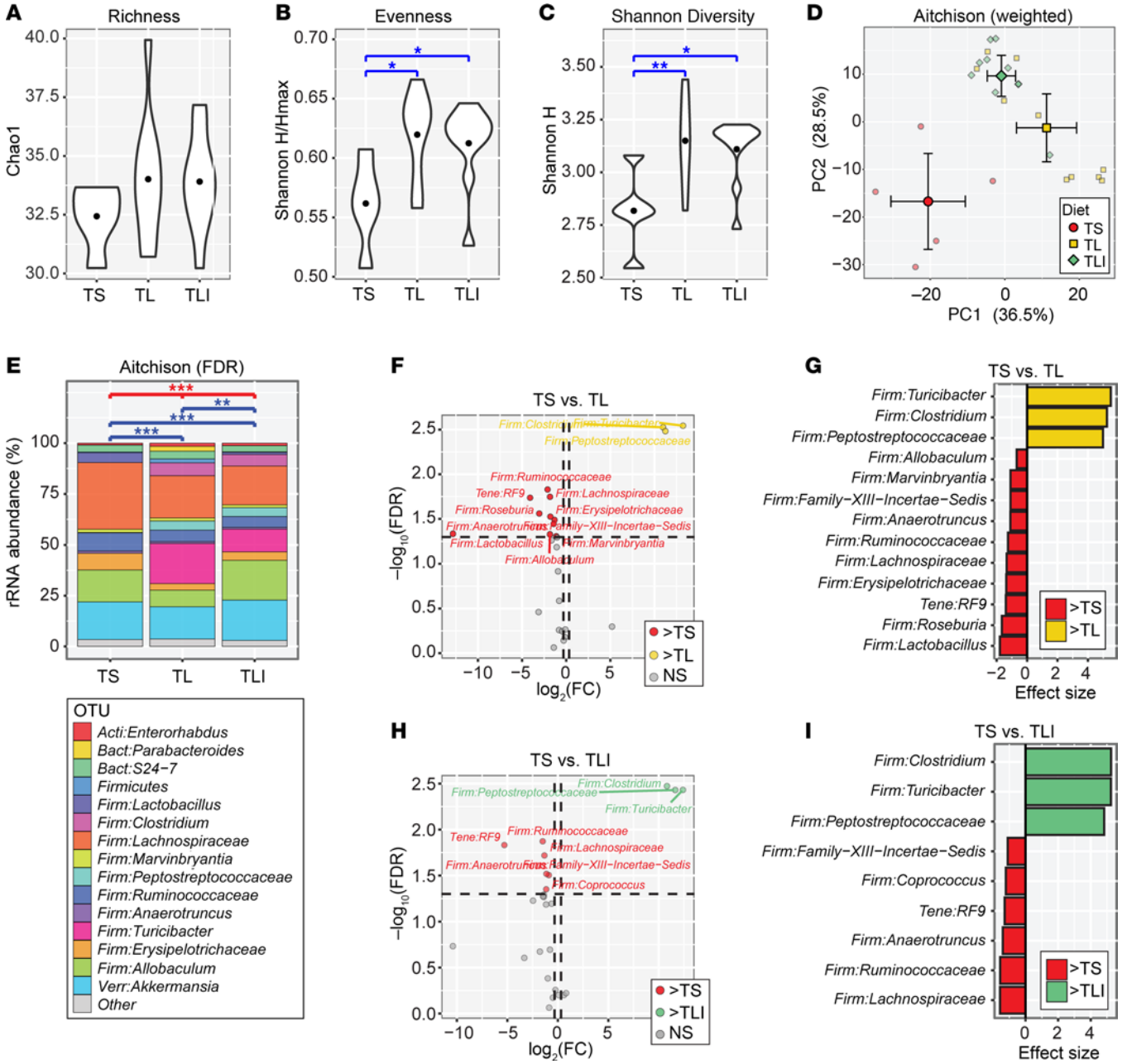

Figure 3. Indole minimally affects bacterial dysbiosis imparted by a TL diet during CIA. Six-week-old male DBA/1 mice were fed a TL or TS diet starting on day –1 and through the duration of the experiment. CIA was induced, and indole (200 μL of a 10 mM solution) or vehicle control (0.33% methanol) was added by oral gavage every other day starting on day 0. On day 35, fecal pellets were harvested, genomic DNA was isolated, and 16S rRNA-Seq was performed to assess microbial diversity for TS+Vehicle (TS, $n = 5$), TL+Vehicle (TL, $n = 10$), and TL+Indole (TLI, $n = 10$). (**A**–**C**) α-Diversity indices are shown for each group. $^{*}P < 0.05$ and $^{**}P < 0.01$, by 1-way ANOVA with pairwise P values determined by Tukey's honest significance difference tests for differences between groups. Richness: measured by the Chao1 index. Shannon Diversity: measured by Shannon's diversity index, H. Evenness: measured by H/Hmax where Hmax = the maximum H for a subject. (**D**) PCA, in which smaller, lighter symbols represent individual mice and large, darker symbols represent group means plus 95% CIs for PC1 and PC2. (**E**) Bar charts showing mean distributions of taxa for each group. Taxa with relative abundances of less than 1.0% were collapsed into the "Other" category to simplify the figure. OTU, operational taxonomic units. Differences in β-diversity between groups were assessed using PERMANOVA tests with the weighted Aitchison dissimilarity index: $^{**}P < 0.01$ and $^{***}P < 0.001$. (**F**–**I**) Volcano and effect size plots generated by ANOVA-like differential expression (ALDEx2) analysis indicate taxa that were significantly enriched or depleted (FDR-corrected P value < 0.05) in mice with CIA on 1 diet compared with another: TS+Vehicle versus TL+Vehicle (**F** and **G**), TL+Vehicle versus TL+Indole (**H** and **I**).

complement deposition in the TL+Vehicle group compared with the TS+Vehicle group, which was restored with indole supplementation (Figure 5B and Supplemental Figure 5, E and F). Furthermore, complement fixation by CII-specific antibodies and C3 deposition in the joint both correlated with CIA severity (Supplemental Figure 5, G and H), providing further evidence that antibody function, rather than concentration, is more important in CIA pathogenesis.

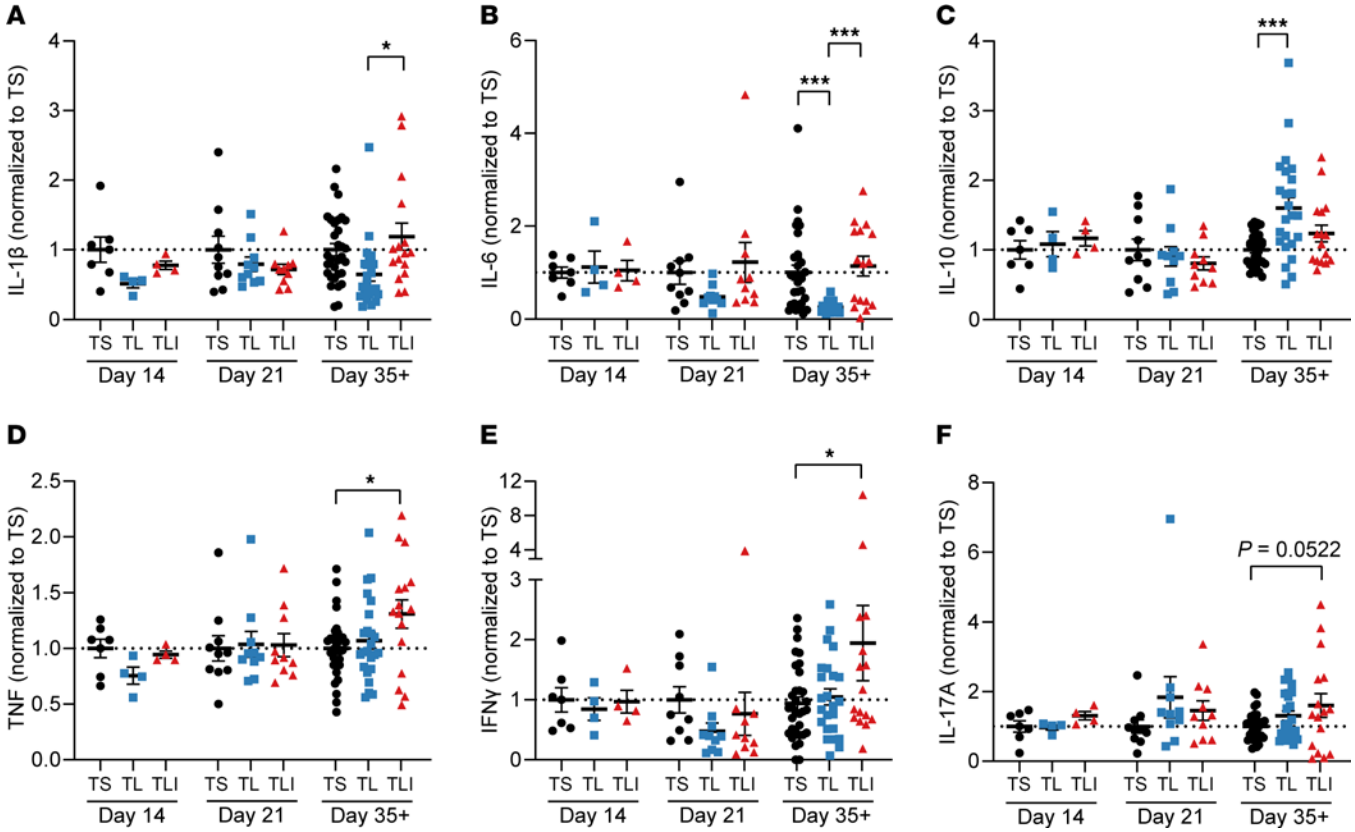

Figure 4. Indole alters the cytokine profile in CIA. Six-week-old male DBA/1 mice were fed a TL or TS diet starting on day –1 and through the duration of the experiment. Following induction of CIA, mice were treated with indole (200 μL of a 10 mM solution) or vehicle control (0.33% methanol) by oral gavage every other day starting on day 0. (**A**–**F**) Terminal serum was collected at days 14 and 21 and at the plateau of disease (days 35–50) from mice with CIA fed a TL or TS diet and treated with indole (200 μL of a 10 mM solution) or vehicle control (0.33% methanol). Sera were analyzed by an 8-plex immunoassay (Meso Scale). To account for experiment-to-experiment variability, serum cytokine concentrations (as denoted on the *y* axis) were normalized to the mean of the TS+Vehicle group for each experiment and time point. n = 4–8 per group (day 14), 10 per group (day 21), and 16–28 per group (days 35–50), pooled from 9 independent experiments and plotted as individual mice (symbols) and the mean ± SEM (bars). $^{*}P < 0.05$ and $^{***}P < 0.001$, by 1-way ANOVA with Bonferroni's correction for multiple comparisons.

We then examined anti-CII IgG isotypes and Fc glycosylation, as both have been shown to affect complement binding (47–52). Whereas we did not observe significant differences in anti–CII IgG1 (Supplemental Figure 6A), the TL+Vehicle treatment significantly reduced anti–CII IgG2a and IgG2b concentrations (Figure 5, C and D). Intriguingly, although indole supplementation was not sufficient to rescue anti–CII IgG2a levels, anti–CII IgG2b levels were restored to those of the TS+Vehicle group (Figure 5, C and D). Furthermore, anti–CII IgG2b levels significantly correlated with CIA severity and complement activation (Supplemental Figure 6, B and C), whereas anti–CII IgG1 levels were only weakly correlated, and IgG2a had no correlation (Supplemental Figure 6, D and E). Because complement-fixing IgG2b has been demonstrated to be highly pathogenic in other models (53), the observed changes in complement activation with indole supplementation may be explained by increased anti–CII IgG2b isotype switching.

We next assessed IgG glycosylation. The N297 residue of the IgG Fc chain is modified by glycans in response to physiological changes. The main IgG-Fc glycoforms are agalactosylated (G0), galactosylated (G1 or G2), or sialylated (S1 or S2) (51, 54) (Figure 5E). IgG-Fc glycosylation patterns are altered in patients with RA, with decreased sialylation compared with controls (55, 56). N-terminal sialic acid residues have been reported to have antiinflammatory properties, specifically through the induction of inhibitory FCγRIIb receptors (57), and can act as a "cap" that blocks complement C1q from binding to galactose residues (46, 47, 52). We first assessed glycosylation of total purified serum IgG from mice with CIA at day 35 by measuring the G0, G1, G2, S1, and S2 glycoforms. The TL+-Vehicle group had significantly reduced galactosylated (G1 + G2) and correspondingly increased sialylated (S1 + S2) IgG levels compared with the TS+Vehicle group (Figure 5, F and G). In a second experiment (plotted separately due to HPLC batch effects), indole supplementation resulted in an intermediate level of IgG sialylation (Supplemental Figure 6, F and G).

We then reasoned that glycosylation may be more profoundly affected in the antigen-specific antibody response and examined glycosylation of purified CII-specific antibodies from day 35 serum. Because of a low yield of CII-IgG after purification, there was a high level of background in the HPLC analysis that prevented us from quantifying the agalactosylated (G0) glycoform. Therefore, we quantified the relative levels of either galactosylated (G1 + G2) or sialylated (S1 + S2) glycoforms. Although there were no statistically significant differences between groups, we observed the same pattern in the CII-specific fraction as that seen with total IgG: the TL+Vehicle group

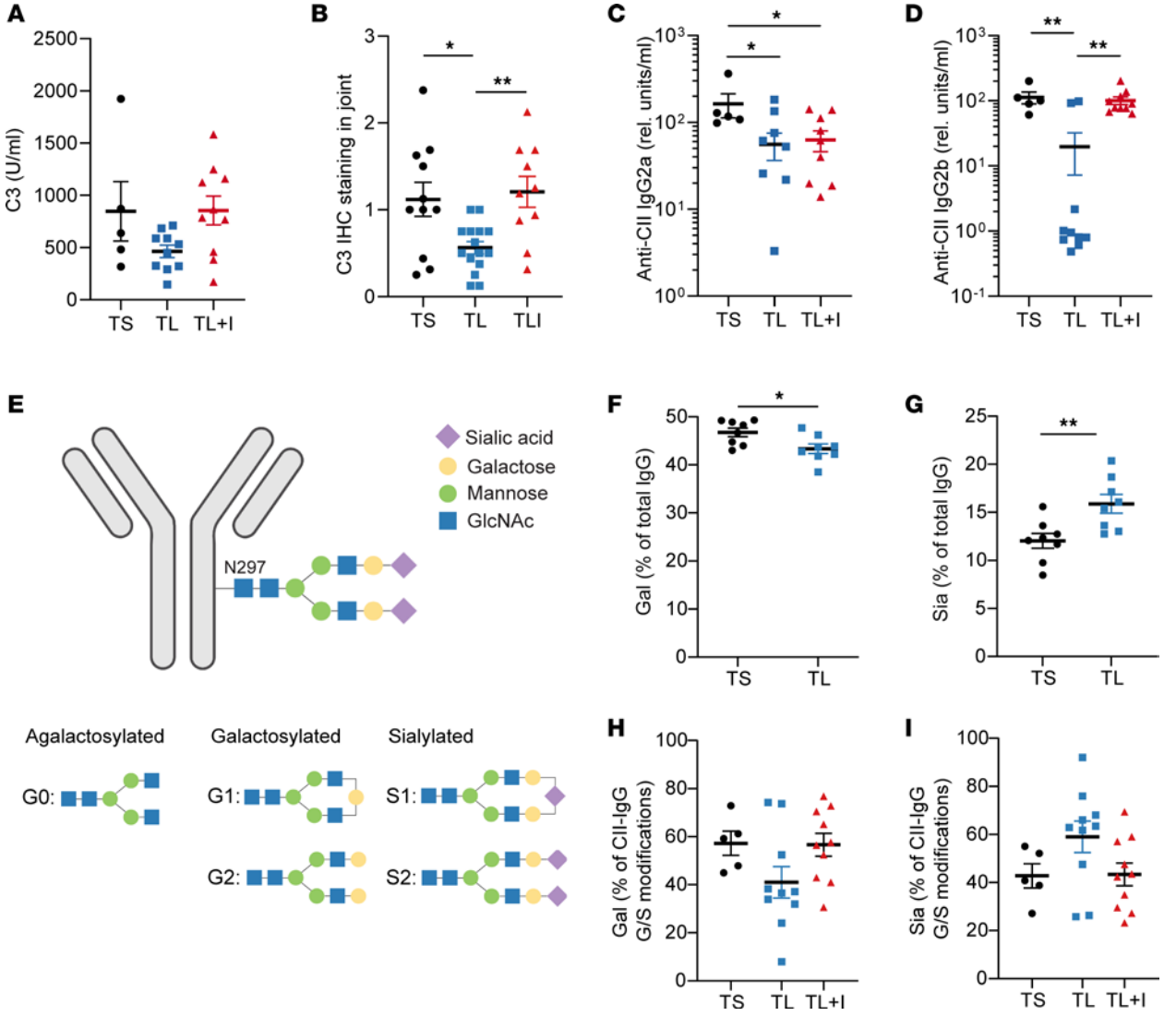

Figure 5. Indole alters complement activation, IgG subclass, and glycosylation. Six-week-old male DBA/1 mice were fed a TL or TS diet starting on day –1 and through the duration of the experiment. Following induction of CIA, mice were treated with indole (200 μL of a 10 mM solution) or vehicle control (0.33% methanol) by oral gavage every other day starting on day 0. (**A**) Day 35 serum was evaluated by ELISA for C3 binding to anti–CII IgG. *n* = 5–10 per group from 1 independent experiment. (**B**) Formalin-fixed, paraffin-embedded (FFPE) joints were stained for complement C3 by immunohistochemistry, and staining intensity was scored. Each data point represents the average complement deposition score of all 4 paws for 1 mouse (maximum score = 3 per paw). *n* = 10–15 per group, pooled from 2 independent experiments. (**C** and **D**) Day 35 serum was evaluated by ELISA for anti–CII IgG2a (**C**) and anti–CII IgG2b (**D**). *n* = 5–10 per group from 1 independent experiment. (**E**) Diagram of possible glycosylation patterns on N297 of the IgG Fc domain. Blue squares denote *N*-acetylglucosamine; green circles denote mannose; yellow circles denote galactose; purple diamonds denote sialic acid. (**F** and **G**) Total IgG was purified from serum, and IgG glycosylation patterns were assessed by LC-MS/MS. The percentage of galactosylation (Gal) and the percentage of sialylation (Sia) are plotted, respectively. Galactosylation and sialylation were calculated as a percentage of all glycoforms (G0, G1, G2, S1, and S2). *n* = 8 per group from 1 independent experiment. (**H** and **I**) In a separate experiment, anti–CII IgG was purified using CII-linked CNBr Sepharose 4B beads. IgG glycosylation patterns were assessed by LC-MS/MS. Galactosylation and sialylation are plotted as the percentage of G1, G2, S1, and S2 glycoforms only. *n* = 5–10 per group from 1 representative experiment. For all panels, values are plotted as individual mice (symbols) and the mean ± SEM (bars). **P* < 0.05, ***P* < 0.01, ****P* < 0.001, and *****P* < 0.0001, by 1-way ANOVA with Bonferroni's correction for multiple comparisons (**A**–**D**, **H**, and **I**) and unpaired Student's *t* test (**F** and **G**). rel., relative.

had decreased galactosylation and increased sialylation compared with the TS+Vehicle group (Figure 5, H and I). Indole supplementation appeared to restore the glycosylation pattern of the TS group but was not statistically significant (Figure 5, H and I). These data suggest that indole may promote pathogenic antibody glycosylation in an antigen-specific manner. Altogether, these findings suggest that the observed increase in complement activation following indole supplementation may be due to isotype switching and/or antibody glycosylation patterns that favor complement binding.

Indole may enhance Th17 immunity. Previous studies have shown that the IL-23/IL-17 axis (Th17), but not the IL-12/IFN-γ (Th1) axis, is required for CIA (58) and that the IL-23/Th17 axis promotes CIA, at least in part, through altered CII-antibody glycosylation (46). On the basis of our observations that indole supplementation led to decreased antibody sialylation (Figure 5I), we hypothesized that indole supplementation may promote CIA through the IL-23/Th17 axis. As such, we first assessed whether $CD4^+$ T cells were affected by indole supplementation. At CIA day

35, splenic total CD4$^+$ T cell numbers were not significantly different between the TL+Vehicle and TS+Vehicle groups, suggesting that reduced dietary Trp in mice with CIA on the TL diet did not alter global T cell numbers (Supplemental Figure 7, A and B). We then assessed the proportions of naive, effector, and central memory CD4$^+$ T cells. The TL+Vehicle diet did not significantly affect the distribution of effector or naive CD4$^+$ T cells (Figure 6, A–C). Surprisingly, there was a significant reduction in the proportion of naive CD4$^+$ T cells in the TL+Indole group and a corresponding increase in effector and central memory cell populations compared with the TL+Vehicle group (Figure 6, A–C). When assessed by cell number, we observed a significant reduction in the total number of naive CD4$^+$ T cells in the TL+Indole group, but no changes in effector or central memory cell numbers (Supplemental Figure 7, C–E). In the colon, there were no significant differences in the proportion of naive, effector, and central memory CD4$^+$ T cells (Supplemental Figure 7, F–H).

Because of the skewed proportions of naive and effector CD4$^+$ T cells observed in the spleen, we next assessed effector CD4$^+$ T cell subsets, including Foxp3$^+$ Tregs and RORγt$^+$ Th17 cells. There were slight increases in FoxP3$^+$CD25$^+$ splenic Tregs in mice on either the TL+Vehicle or TL+Indole diet compared with TS+-Vehicle (Figure 6D) and an approximately 2-fold increase in the percentage of RORγt$^+$FoxP3$^-$ splenic Th17 cells in the TL+Indole group compared with the TL+Vehicle group (Figure 6E), ultimately leading to an increased Th17/Treg ratio by both percentage (Figure 6F) and cell number (Supplemental Figure 8, A–C). These same trends were observed in colon T cells as well (Supplemental Figure 8, D–F), suggesting a potential local (gut) and systemic (spleen) impact of Trp metabolism on Tregs and indole-stimulated skewing of Th17 cells. The skewed splenic Th17/Treg ratio was only observed at CIA day 35, but not day 21 (Figure 6F), suggesting that the systemic Th17 response may be amplified following secondary immunization. Furthermore, restimulation of splenocytes harvested on day 35 with CII led to significantly higher IL-17 production in the TL+Indole group compared with TL+Vehicle group (Figure 6G). Although the trends were the same for stimulation with anti-CD3/CD28 beads (Figure 6H), the difference in IL-17 production between the groups was more pronounced with CII stimulation, suggesting a role for antigen-specific IL-17 production. There were no detectable differences in other Th17-related cytokines including IL-21 (below the limit of detection) and IL-22, although there was a trend toward increased GM-CSF in the TL+Indole group (Supplemental Figure 8, G–L). Overall, these findings suggest that indole may either directly or indirectly skew the effector T cell response in CIA.

Our data thus far suggested that indole affected autoantibody sialylation, IgG2b production, and Th17 cellular responses. Because IL-23 has been shown to mediate Th17-derived IL-21 and IL-22 to enhance antibody pathogenicity via decreased sialylation of CII-specific antibodies (46), we hypothesized that indole mediates CIA induction through IL-23. To test this hypothesis, TL+Indole mice were given anti–IL-23p19 or an isotype control antibody weekly during preclinical CIA (days 0–21). As observed previously in CIA (59), anti–IL-23p19 treatment resulted in a significant reduction in CIA severity compared with isotype control antibody in TL+Indole mice (Figure 6I). Together, these data provide preliminary evidence that indole acted through the IL-23/Th17 axis to incite disease via modulation of the autoantibody response.

Indole stimulation induces similar pathways in human intestinal mononuclear cells. Finally, we tested whether indole could induce similar pathways in humans as well as mice. We rationalized that, because indole is produced by the gut microbiome and absorbed through the gut, intestinal lymphocytes are more likely to interact with indole compared with circulating lymphocytes and that testing the effects of indole on human colon mononuclear cells would be most physiologically relevant. We obtained LPMCs from macroscopically normal, discarded colon tissues obtained during bowel resection surgeries (60–62). LPMCs from 5 donors were individually stimulated with 1 mM indole or vehicle. After 4 hours, CD3$^+$ T cells and CD19$^+$ B cells were flow sorted from the pooled stimulation, RNA was extracted and sequenced, and Ingenuity Pathway Analysis was performed to identify differentially expressed pathways following indole stimulation compared with vehicle.

In the CD19$^+$ B cell subset (Figure 7A, Supplemental Table 1, and Supplemental Figure 9), there were 21 pathways that were significantly enriched ($P < 0.05$) and that were predicted to be significantly activated or repressed (z score >|2|). Of these pathways, "IL-17 signaling" had the highest z score ($z = 4.36$, $P = 0.02$), while "UDP-*N*-acetyl-D-glucosamine biosynthesis II", which produces the glycosylation precursor *N*-acetylglucosamine (GlcNAc), was the most statistically significant ($z = 2$, $P = 0.0002$). "NRF2-mediated oxidative stress response," "HIF1α signaling," "unfolded protein response," and "p38 MAPK signaling" were among the other most significantly affected pathways. In the CD3$^+$ T cell subset (Figure 7B, Supplemental Table 2, and Supplemental Figure 10), 3 pathways were significantly enriched and activated: "IL-17 signaling" ($z = 3.87$, $P = 0.018$), "differential regulation of cytokine production in intestinal epithelial cells by IL-17A and IL-17F" ($z = 2.24$, $-P = 0.003$), and "neuroprotective role of THOP1 in Alzheimer's disease" ($z = 2.7$, $P = 0.006$). The "neuroprotective role of THOP1 in Alzheimer's disease" pathway was primarily driven by increased expression of endonucleases and serine proteases (Supplemental Table 2). Together, these data provide proof of concept that the observed indole-mediated effects on Th17 immunity, antibody glycosylation, and altered class switch recombination in mice with CIA may also be relevant for human intestinal immunity.

Discussion

Although there is compelling evidence for a mucosal origins hypothesis for RA and SpA, the mechanisms by which microbes contribute to the induction of autoimmunity remain elusive. There are several potential processes by which specific microbes could stimulate the development of autoimmunity, including altered production of bacterial metabolites, many of which have immunomodulatory functions (25–27). Our observations of elevated Trp-derived indoles in 2 independent murine models of inflammatory arthritis (CIA and *Subdoligranulum isolate 7*–induced arthritis), as well as in patients with SpA (9), prompted us to investigate the requirement for indole in the development of CIA as a model in which cause-effect could be established. Because indole is exclusively produced from microbial metabolism of dietary Trp, we modulated indole production

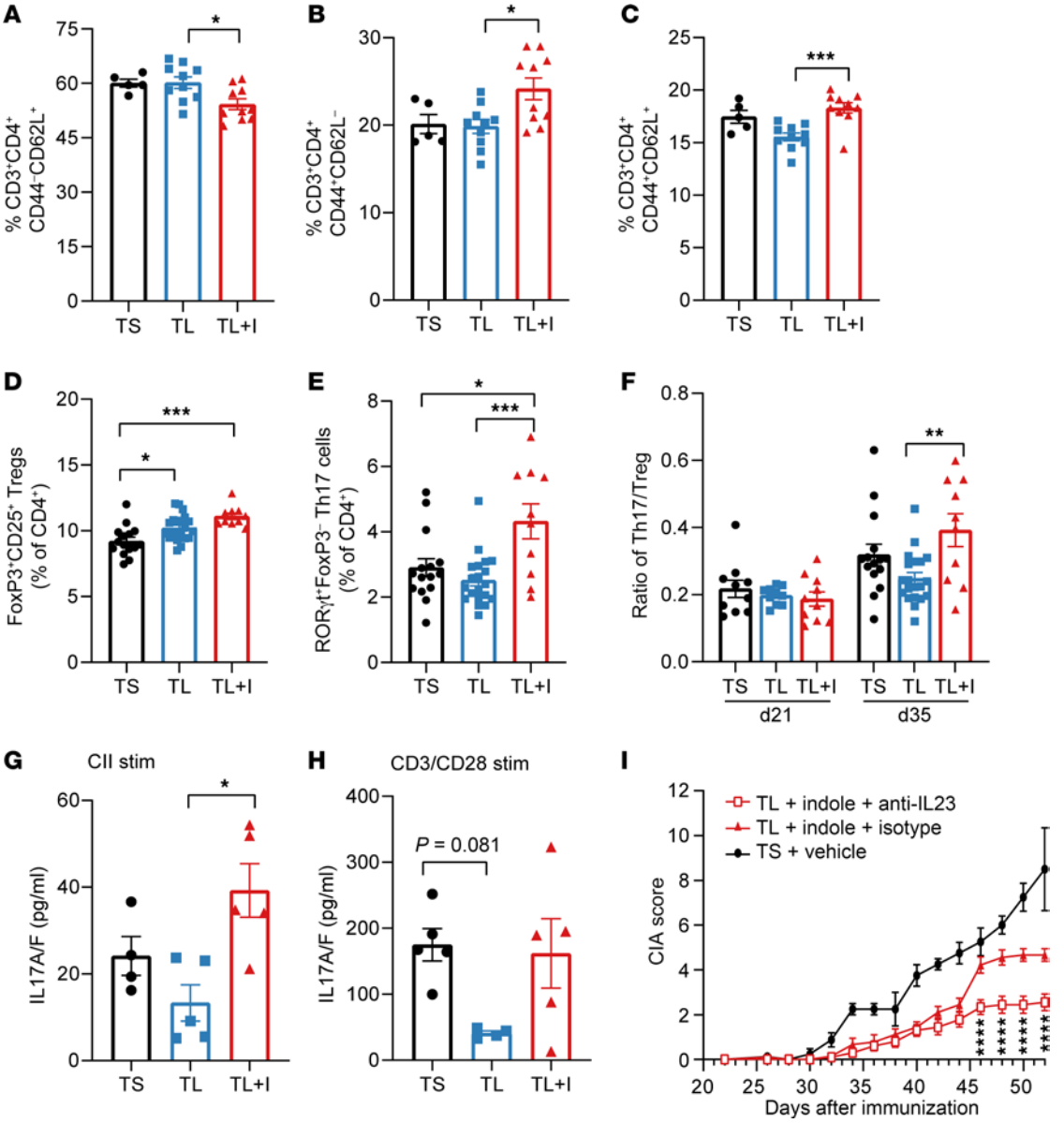

Figure 6. Indole skews toward Th17 cells. Six-week-old male DBA/1 mice were fed a TL or TS diet starting on day –1 and through the duration of the experiment. Following induction of CIA, mice were treated with indole (200 μL of a 10 mM solution) or vehicle control (0.33% methanol) by oral gavage every other day starting on day 0. Spleens were harvested on day 35 for analysis by flow cytometry. (**A**) Splenic naive ($CD44^-CD62L^+$) T cells as a percentage of $CD4^+$ T cells. (**B**) Splenic effector T cells ($CD44^+CD62L^-$) as a percentage of $CD4^+$ T cells. (**C**) Splenic central memory T cells ($CD44^+CD62L^+$) as a percentage of $CD4^+$ T cells. n = 5–10 per group from 1 independent experiment for **A**–**C**. (**D**) Splenic $FoxP3^+ROR\gamma t^-CD25^+$ Tregs are plotted as a percentage of total $CD4^+$ T cells. (**E**) Splenic $CD3^+CD4^+FoxP3^-ROR\gamma t^+$ Th17 cells are plotted as a percentage of total $CD4^+$ T cells. (**F**) Ratio of splenic Th17 to Tregs at CIA days 21 and 35. n = 10–20 per group, pooled from 2 independent experiments (day 35 [d35]) (**D**–**F**) and n = 10 per group (day 21 [d21]) from 1 independent experiment (**F**). (**G** and **H**) Total splenocytes from CIA day 35 were harvested and restimulated (stim) with bovine type II collagen (**G**) or CD3/CD28 Dynabeads (**H**); supernatant was saved and IL-17A/F was measured by Meso Scale Discovery (MSD). One statistical outlier was identified in the TS+Vehicle group using Grubb's test and was excluded from analysis. n = 4 (TS+Vehicle) and n = 5 (TL+Indole, TL+Vehicle) per group from 1 independent experiment. (**I**) TL+Indole-treated mice received i.p. injections of 100 μg anti–IL-23p19 or isotype (anti-HRP) on CIA days 0, 7, 14, and 21, and CIA severity was monitored. n = 10 (TL+Indole+anti–IL-23), n = 10 (TL+Indole+Isotype), and n = 4 (TS+Vehicle). Asterisks show the comparison between TL+Indole+Isotype versus TL+Indole+anti–IL-23. For all panels, values are plotted as individual mice (symbols) and the mean ± SEM (bars). $^*P < 0.05$, $^{**}P < 0.01$, $^{***}P < 0.001$, and $^{****}P < 0.0001$, by 1-way ANOVA with Bonferroni's correction for multiple comparisons (**A**–**H**) or 2-way ANOVA with Bonferroni's correction for multiple comparisons (**I**).

through either antibiotic-mediated microbiome depletion or reduction of dietary Trp. Depletion of either the microbiome or dietary Trp protected mice from developing CIA, and adding back indole rescued CIA severity, suggesting that indole was sufficient to incite disease. These findings were further confirmed by amelioration of disease in mice colonized with tryptophanase-deficient bacteria, which are unable to produce indole.

While altered Trp metabolism signatures have been observed in systemic lupus erythematosus (SLE), SpA, and RA (9, 22, 31–35, 63), as well as in murine lupus and EAE models

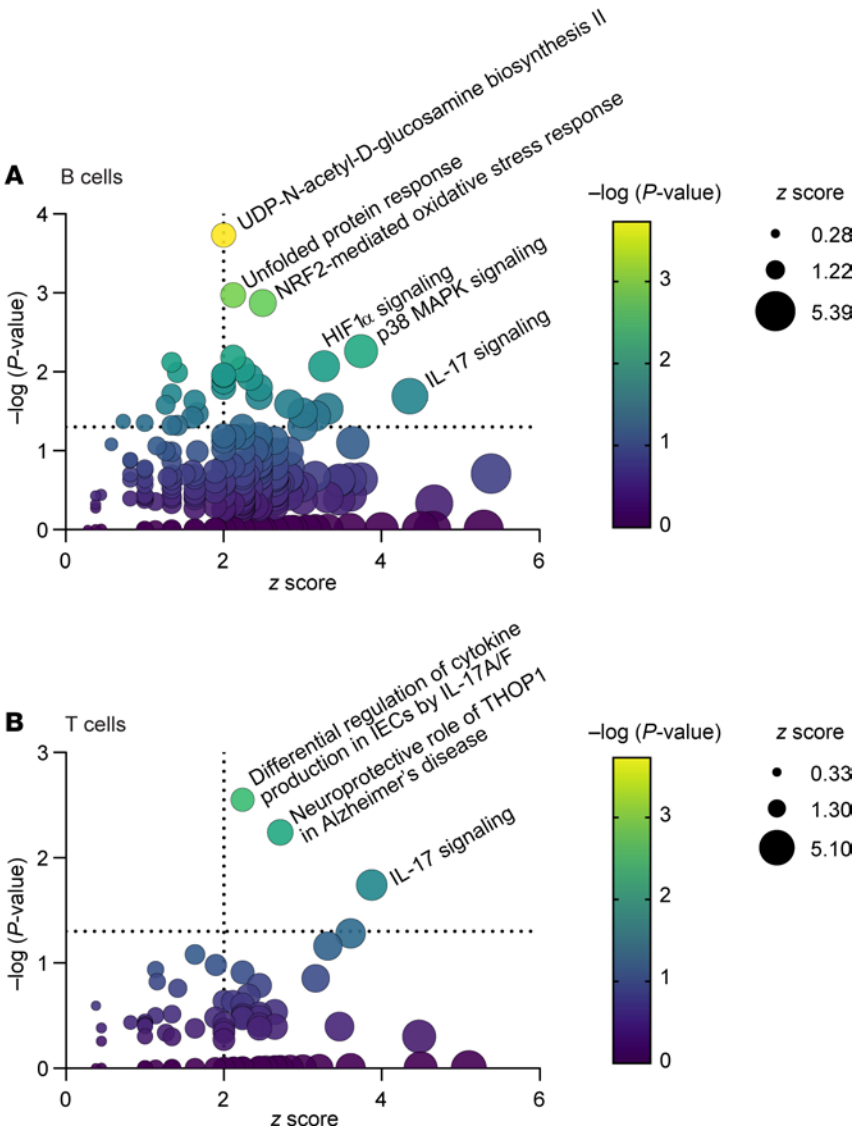

Figure 7. Indole-stimulated human intestinal cells also highlight changes in function. LPMCs isolated from healthy human colon tissue were stimulated with 1 mM indole or vehicle for 4 hours. CD19⁺ B cells and CD3⁺ T cells were flow sorted, and RNA was isolated for RNA-Seq. Differentially expressed pathways (indole versus vehicle) were identified with Ingenuity Pathway Analysis for (**A**) CD19⁺ B cells and (**B**) CD3⁺ T cells. *n* = 5 paired samples.

(20, 29), there are conflicting roles for Trp metabolites in RA and experimental arthritis models. IAA, 5-hydroxytryptophan (5-HTP), and 5-HIAA ameliorate arthritis severity in proteoglycan-induced spondyloarthritis (64), CIA (65), and antigen-induced arthritis (66), respectively. Studies of kynurenine supplementation, or inhibition of kynurenine production with the IDO1 inhibitor 1-methyl-tryptophan (1-MT) have shown conflicting effects on arthritis severity: 1-MT treatment ameliorates disease in the K/BxN (67) murine model but exacerbates disease in the CIA model (68). Intra-articular injection of indole, but not kynurenine, into rabbit knees induced RA-like synovitis (69). Furthermore, these metabolites are either exclusively host derived (5-HIAA), or can be produced by either the host or the microbiome (IAA, 5-HTP, kynurenine). Thus, there is a great need to understand the specific role of tryptophan metabolism and microbiome-derived metabolites in the development of autoimmune arthritis.

Despite the conflicting role of Trp metabolites in arthritis models, our study is in agreement with recent findings that a TL diet protects against disease in murine models of EAE and lupus (20, 29). While Trp can be metabolized by both host and microbial enzymes, our study provides evidence that microbial, rather than host, metabolism of Trp plays a major role in the development of CIA, in agreement with what has previously been shown in models of SLE and EAE (29, 70, 71). However, despite the consilience of these findings, it appears that the specific Trp metabolites that potentiate disease may be unique to each model. Because each of these disease models has been shown to be microbiome dependent, the unique dysbiosis of each model may lead to differential production of Trp metabolites by the microbiota and thereby potentiate disease via distinct mechanisms: in lupus-prone triple congenic *B6.Sle1.Sle2.Sle3* (TC) mice, elevated levels of serum kynurenine appear to impair Treg function (20). Although kynurenine is thought to be primarily produced by host

metabolism of Trp via indoleamine-2,3-dioxygenase (IDO1), the microbiota can also produce kynurenine via tryptophan-2,3-dioxygenase (TDO2) (72). Choi et al. (20) showed that antibiotic treatment, but not IDO1 inhibition, reduces serum kynurenine levels, suggesting that dysbiosis in TC mice leads to increased microbe-derived kynurenine that may promote disease development (20). Alternatively, in an EAE model in which disease severity is exacerbated by colonization with *Lactobacillus reuteri*, Trp metabolism by microbial aromatic amino acid aminotransferase (ArAT) and aliphatic amidase E (AmiE) was increased in a Trp- and microbiome-dependent manner (29). While both studies identified Trp metabolites that are correlated with disease severity and showed that they can potentiate pathogenic T cell function in vitro, they did not test whether these metabolites directly incite disease in vivo. In our study, we demonstrate the specific requirement for a Trp-derived metabolite in the development of CIA. Whether other indole-related metabolites can function similarly to indole in the CIA model or whether indole in the context of a complex metabolome will have similar effects will be essential to better understand the effects of Trp metabolites on host immunity both alone and in combination.

In our studies, we did not identify a specific indole-producing species that incites disease, but rather demonstrated a significant correlation between many taxa that were expanded in our CIA studies (*Firmicutes*, *Barnesiella*, *Rikenellaceae*, *Lactobacillales*) and indole levels. These taxa, as well as others that have been shown to be expanded in CIA (such as *Lachnospiraciae* and *Lactobacillaeae*; refs. 18, 19), RA (*Lachnospiraceae bacterium, lactobacillus spp.*, *Faecalibacterium*; refs. 73, 74), and SpA (*Ruminococcaceae*, *Rikenellaceae*, *Porphyromonadaceae*, *Bacteroidaceae*, *Lachnospiraceae*; ref. 4) are either predicted or known to produce indole (via TrpNet.ca), providing candidate bacteria for further study. Linking the essential indole-producing microbes to the development of inflammatory arthritis may provide a new therapeutic opportunity.

CIA is a multifaceted disease model. While CII-reactive autoantibodies that bind to cartilage and activate complement are the primary pathologic drivers of disease (44, 45), CII-reactive B cells, $CD4^+$ T cells, and proinflammatory cytokines are also required for disease development. Indole supplementation appears to affect several aspects of CIA pathophysiology, including the induction of proinflammatory cytokines, $CD4^+$ T cell skewing toward Th17 cells, and antibody-mediated complement activation. As the specific cellular target or targets of indole have not yet been identified, it is difficult to dissect which of these effects are directly initiated by indole stimulation and which effects are secondary to an indole-induced proinflammatory environment. Furthermore, while our studies suggest that indole had minimal effects on microbiome composition, we cannot definitively rule out the possibility that indole supplementation altered the microbiome. Despite this limitation, the magnitude (effect size) of the microbiome changes observed with the TS versus TL diets was much higher compared with the differences between TL+Vehicle and TL+Indole, suggesting that indole supplementation had a much stronger effect on host immunity than it did on the microbiome.

Despite these confounding factors, our findings allow us to construct a hypothesized mechanism through which indole acts. We show increased complement deposition in the joints of indole-supplemented CIA mice and increased complement activation by CII-specific antibodies. Our data suggest that indole enhanced complement activation through 2 mechanisms: skewed CII-specific antibody isotype switching and glycosylation. First, indole restored CII-specific IgG2b production. Complement activation has been shown to differ by isotype, with IgG2b ≥IgG2a >IgG1 (48–50). Analysis of high-affinity antierythrocyte autoantibodies demonstrated that IgG2b antibodies had a greater than 200-fold increase in pathogenicity compared with other isotypes, which was almost entirely due to complement activation (53). As such, the indole-mediated rescue of IgG2b production may explain the increase in complement fixation observed in anti-CII antibodies from the TL+Indole group.

Second, indole appears to alter antibody glycosylation. IgG-Fc sialylation acts as a protective "cap" to prevent complement binding to galactose residues. The ratio of galactosylated/sialylated residues was increased in CII-specific antibodies from indole-supplemented mice, which may also explain the increase in complement fixation observed in anti-CII antibodies from the TL+Indole group. A prior study linked CII-antibody sialylation to IL-17–independent Th17 cellular responses during CIA: IL-23 stimulation of Th17 cells induces decreased IgG-Fc sialylation via decreased expression of *St6gal1* in B cells (46). A similar study showed that IgG-Fc desialylation promotes nephropathy in an SLE mouse model in an IL-17A– and IL-23–dependent manner (75). We have previously shown that antibiotic-mediated protection from CIA is due, at least in part, to increased IgG-Fc sialylation, suggesting a role for microbiome-mediated changes in IgG-Fc sialylation (18). As such, one possible explanation for our data is that microbiome-derived indole promotes IL-23/Th17–mediated changes in antibody glycosylation. To support this explanation, we show that IL-23 blockade ameliorated disease in the indole-CIA model, suggesting that indole may act upstream of T cells, such as on IL-23–producing DCs. The observed expansion of Th17 cells in the indole-supplemented group and the requirement for IL-23 in indole-mediated CIA provide further evidence for an effect of indole on the IL-23/Th17 axis in CIA. Furthermore, although the signals leading to IgG2b class switch recombination have not been well characterized in vivo, 1 study showed that IgG2b class switch recombination is decreased in IL-23p19$^{-/-}$ mice via decreased Tfh17 cells (76). Altogether, these supporting data and ours suggest a mechanism in which indole induces pathogenic antibody formation through class switching to IgG2b as well as decreased antibody sialyation that enhances complement fixation, and that these changes may occur through the IL-23/Th17 axis. Whether (and how) Th17 cells directly affect antibody function in the indole-CIA model is yet to be determined, as prior studies have shown an IL-17–independent but IL-21– and IL-22–dependent role of Th17 cells in antibody glycosylation (46).

We also provide proof of concept that indole-mediated activation of immune cells may occur in humans as well. The pathways that were upregulated in human colon lymphocytes following indole stimulation paint a picture of Th17 cell and plasma cell activation, similar to what we observed in mice with CIA: "IL-17 signaling" (which was upregulated in both B and T cells) promotes B cell differentiation and plasma cell formation. "HIF1α signaling" and "NRF2-mediated oxidative stress response"

were also upregulated in B cells: hypoxic environments induce HIF1α and NRF2, which then promote plasma cell formation (77); the unfolded protein response (which was also upregulated in B cells) is upregulated during plasma cell differentiation to accommodate increased antibody production (78). Furthermore, it has been shown that IL-17 signaling can sustain the plasma cell response via p38/MAPK signaling in B cells from patients with lupus (79), and p38-MAPK signaling (upregulated in B cells) also regulates class-switch recombination (80). Finally, in concordance with our findings, individuals with RA have aberrant total IgG glycosylation that increases as these individuals transition from the at-risk stage to disease and that correlates with disease activity (81), as well as an increased Th17 signature (82–86). While further studies are required to validate which pathway(s) and genes are indeed upregulated following indole stimulation, and whether indole and primarily affects intestinal immunity (serving as a mucosal trigger) or systemic immunity (i.e., by exacerbating joint pathology), these data provide proof of concept that the increased Th17 signature and altered antibody patterns observed in CIA and indole-stimulated LPMCs may also be relevant to human disease.

Altogether, our study provides one potential mechanism by which the microbiome directly contributes to the development of autoimmunity and lays the groundwork for future mechanistic studies on the effect of indole on the IL-23/Th17 axis and autoantibody pathogenicity, and suggests potential for blocking indole production as a therapy for RA and SpA.

Methods

Detailed methods can be found in the Supplemental Methods.

Data availability. Sequencing data from these studies have been deposited in publicly accessible databases. The 16S data can be found in the Sequencing Read Archive (SRA) BioProject database (PRJNA1004672). The RNA-Seq data can be found in the NCBI's Gene Expression Omnibus (GEO) database (GEO GSE241655). Values for all data points in the figures are provided in the Supplemental Supporting Data Values file.

Statistics. Unless specified otherwise, data were analyzed using GraphPad Prism (GraphPad Software); specific statistical tests for comparisons are referenced in the figure legends. For comparisons between groups, 1-way ANOVA with Bonferroni's correction for multiple comparisons was used if there were more than 2 groups being compared; a 2-tailed Student's *t* test was used for comparison between 2 groups. To score CIA severity between groups across several time points, a 2-way ANOVA with Bonferroni's correction for multiple comparisons was used. Pearson's correlation with 2-tailed *P* value was used for all correlations. For all statistical comparisons, a *P* value of less than 0.05 was considered statistically significant. The data in the figures are presented as the mean ± SEM.

Study approval. All animal studies were approved by the IACUC of the University of Colorado School of Medicine (protocol no. 173). Research associated with the use of LPMCs was reviewed by the Colorado Multiple Institutional Review Board (COMIRB protocol no. 17-0977) at the University of Colorado Anschutz Medical Campus and deemed "Not Human Subject Research," as defined by their polices in accordance with OHRP and FDA regulations.

Author contributions

BJS, BT, WKJ, and KAK designed the project, performed the experiments, and analyzed the data. BJS and KAK assembled the data and wrote the manuscript. BA, JT, AS, SL, MEC, and SF contributed to data acquisition and analysis. AO, EEA, and SPC ran and analyzed the metabolites studies. DNF, JMK, and CER ran and analyzed the microbiome studies. ASD and SPC provided the *E. coli* mutants. SLS and RMA ran and analyzed the glycosylation studies. AJB, AS, SMD, and CCW procured, processed, and acquired and analyzed data for the human LPMC studies. All authors reviewed the manuscript and approved its final submitted version.

Acknowledgments

The work by the authors is supported through the National Institute of Arthritis and Musculoskeletal and Skin Diseases (NIAMS), NIH (R01AR075933, to KAK; P30AR079369, and T32AR007534, to WKJ, BT, AJB, MEC, and SF); the National Institute of Allergy and Infectious Diseases (NIAID), NIH (T32AI007405 and F30AI174817, to BJS); and the Rheumatology Research Foundation Future Physician Scientist Award (to BJS and MEC) and the Scientist Development Award (to AJB). We would like to acknowledge the following CU Cancer Center Support Grant–funded (NIH P30CA06934) shared resource cores: Research Histology Core (RRID:SCR_021994); Flow Cytometry Shared Resource Core (RRID:SCR_022035); Mass Spectrometry Metabolomics Shared Resource Facility (RRID:SCR_021988); and the Genomics/Microarray Core (RRID:SCR_021984). We also acknowledge the Barbara Davis Center Cell and Tissue Analysis Core at the University of Colorado Diabetes Research Center (National Institute of Diabetes and Digestive and Kidney Diseases [NIDDK], NIH, P30DK116073).

Address correspondence to: Kristine A. Kuhn, University of Colorado School of Medicine, 1775 Aurora Ct., Mail Stop B115, Aurora, Colorado 80045, USA. Phone: 303.724.8258; Email: kristine.kuhn@cuanschutz.edu.

1. Yu X-H, et al. Systematic evaluation of rheumatoid arthritis risk by integrating lifestyle factors and genetic risk scores. *Front Immunol*. 2022;13:901223.
2. Li Z, et al. Polygenic risk scores have high diagnostic capacity in ankylosing spondylitis. *Ann Rheum Dis*. 2021;80(9):1168–1174.
3. Deane KD, et al. Genetic and environmental risk factors for rheumatoid arthritis. *Best Pract Res Clin Rheumatol*. 2017;31(1):3–18.
4. Clemente JC, et al. The role of the gut microbiome in systemic inflammatory disease. *BMJ*. 2018;360:j5145.
5. Maeda Y, et al. Dysbiosis contributes to arthritis development via activation of autoreactive T cells in the intestine. *Arthritis Rheumatol*. 2016;68(11):2646–2661.
6. Maeda Y, Takeda K. Host-microbiota interactions in rheumatoid arthritis. *Exp Mol Med*. 2019;51(12):1–6.
7. Rooney CM, et al. Perturbations of the gut microbiome in anti-CCP positive individuals at risk of developing rheumatoid arthritis. *Rheumatology (Oxford)*. 2020;60(7):3380–3387.
8. Koh JH, et al. Factors associated with the composition of the gut microbiome in patients with established rheumatoid arthritis and its value for predicting treatment responses. *Arthritis Res Ther*. 2023;25(1):32.
9. Berlinberg AJ, et al. Multi 'omics analysis of intes-

tinal tissue in ankylosing spondylitis identifies alterations in the tryptophan metabolism pathway. *Front Immunol*. 2021;12:587119.
10. Costello M-E, et al. Brief report: intestinal dysbiosis in ankylosing spondylitis. *Arthritis Rheumatol*. 2015;67(3):686–691.
11. Holers VM, et al. Rheumatoid arthritis and the mucosal origins hypothesis: protection turns to destruction. *Nat Rev Rheumatol*. 2018;14(9):542–557.
12. Wilson TM, et al. Microbial influences of mucosal immunity in rheumatoid arthritis. *Curr Rheumatol Rep*. 2020;22(11):83.
13. Garabatos N, Santamaria P. Gut microbial antigenic mimicry in autoimmunity. *Front Immunol*. 2022;13:873607.
14. Alpizar-Rodriguez D, et al. Prevotella copri in individuals at risk for rheumatoid arthritis. *Ann Rheum Dis*. 2019;78(5):590–593.
15. Chriswell ME, et al. Clonal IgA and IgG autoantibodies from individuals at risk for rheumatoid arthritis identify an arthritogenic strain of Subdoligranulum. *Sci Transl Med*. 2022;14(668):eabn5166.
16. Brakenhoff LKPM, et al. The joint-gut axis in inflammatory bowel diseases. *J Crohns Colitis*. 2010;4(3):257–268.
17. Gracey E, et al. Revisiting the gut-joint axis: links between gut inflammation and spondyloarthritis. *Nat Rev Rheumatol*. 2020;16(8):415–433.
18. Jubair WK, et al. Modulation of inflammatory arthritis in mice by gut microbiota through mucosal inflammation and autoantibody generation. *Arthritis Rheumatol*. 2018;70(8):1220–1233.
19. Liu X, et al. Role of the gut microbiome in modulating arthritis progression in mice. *Sci Rep*. 2016;6(1):30594.
20. Choi S-C, et al. Gut microbiota dysbiosis and altered tryptophan catabolism contribute to autoimmunity in lupus-susceptible mice. *Sci Transl Med*. 2020;12(551):eaax2220.
21. Wang Q, Xu R. Data-driven multiple-level analysis of gut-microbiome-immune-joint interactions in rheumatoid arthritis. *BMC Genomics*. 2019;20(1):124.
22. Yu D, et al. The gut microbiome and metabolites are altered and interrelated in patients with rheumatoid arthritis. *Front Cell Infect Microbiol*. 2022;11:763507.
23. He J, et al. Intestinal butyrate-metabolizing species contribute to autoantibody production and bone erosion in rheumatoid arthritis. *Sci Adv*. 2022;8(6):eabm1511.
24. Luo Y, et al. Alteration of gut microbiota in high-risk individuals for rheumatoid arthritis is associated with disturbed metabolome and initiates arthritis by triggering mucosal immunity imbalance. *Arthritis Rheumatol*. 2023;75(10):1736–1748.
25. Kim CH. Immune regulation by microbiome metabolites. *Immunology*. 2018;154(2):220–229.
26. Atarashi K, et al. Induction of colonic regulatory T cells by indigenous Clostridium species. *Science*. 2011;331(6015):337–341.
27. Ansaldo E, et al. Control of immunity by the microbiota. *Annu Rev Immunol*. 2021;39(1):449–479.
28. Lu Y, et al. TrpNet: understanding tryptophan metabolism across gut microbiome. *Metabolites*. 2021;12(1):10.
29. Montgomery TL, et al. *Lactobacillus reuteri* tryptophan metabolism promotes host susceptibility to CNS autoimmunity. *Microbiome*. 2022;10(1):198.
30. Banoglu E, et al. Hepatic microsomal metabolism of indole to indoxyl, a precursor of indoxyl sulfate. *Eur J Drug Metab Pharmacokinet*. 2001;26(4):235–240.
31. Schroecksnadel K, et al. Increased degradation of tryptophan in blood of patients with rheumatoid arthritis. *J Rheumatol*. 2003;30(9):1935–1939.
32. Forrest CM, et al. Kynurenine and neopterin levels in patients with rheumatoid arthritis and osteoporosis during drug treatment. *Adv Exp Med Biol*. 2003;527:287–295.
33. Pongratz G, et al. Tryptophan metabolism in rheumatoid arthritis is associated with rheumatoid factor and predicts joint pathology evaluated by the rheumatoid arthritis MRI score (RAMRIS). *Clin Exp Rheumatol*. 2019;37(3):450–457.
34. Li J, et al. LC-MS-based serum metabolomics reveals a distinctive signature in patients with rheumatoid arthritis. *Clin Rheumatol*. 2018;37(6):1493–1502.
35. Labadarios D, et al. Metabolic abnormalities of tryptophan and nicotinic acid in patients with rheumatoid arthritis. *Rheumatol Rehabil*. 1978;17(4):227–232.
36. Yanofsky C, et al. The complete nucleotide sequence of the tryptophan operon of Escherichia coli. *Nucleic Acids Res*. 1981;9(24):6647–6668.
37. Newton WA, Snell EE. Catalytic properties of tryptophanase, a multifunctional pyridoxal phosphate enzyme. *Proc Natl Acad Sci U S A*. 1964;51(3):382–389.
38. Phillips RS. Mechanism of tryptophan indole-lyase: insights from pre-steady-state kinetics and substrate and solvent isotope effects. *J Am Chem Soc*. 1989;111(2):727–730.
39. Alexeev EE, et al. Microbiota-derived indole metabolites promote human and murine intestinal homeostasis through regulation of interleukin-10 receptor. *Am J Pathol*. 2018;188(5):1183–1194.
40. Lee J-H, Lee J. Indole as an intercellular signal in microbial communities. *FEMS Microbiol Rev*. 2010;34(4):426–444.
41. Ye L, et al. Interleukin-10 attenuation of collagen-induced arthritis is associated with suppression of interleukin-17 and retinoid-related orphan receptor γt production in macrophages and repression of classically activated macrophages. *Arthritis Res Ther*. 2014;16(2):R96.
42. Alonzi T, et al. Interleukin 6 is required for the development of collagen-induced arthritis. *J Exp Med*. 1998;187(4):461–468.
43. Joosten LAB, et al. Anticytokine treatment of established type II collagen-induced arthritis in DBA/1 mice: a comparative study using anti-TNFalpha, anti-IL-1alpha/beta and IL-1Ra. *Arthritis Rheum*. 1996;58(2 suppl):S110–S122.
44. Holmdahl R, et al. Characterization of the antibody response in mice with type II collagen-induced arthritis, using monoclonal anti-type II collagen antibodies. *Arthritis Rheum*. 1986;29(3):400–410.
45. Nandakumar KS, et al. Collagen type II-specific monoclonal antibody-induced arthritis in mice: description of the disease and the influence of age, sex, and genes. *Am J Pathol*. 2003;163(5):1827–1837.
46. Pfeifle R, et al. Regulation of autoantibody activity by the IL-23-T_H17 axis determines the onset of autoimmune disease. *Nat Immunol*. 2017;18(1):104–113.
47. Peschke B, et al. Fc-galactosylation of human immunoglobulin gamma isotypes improves C1q binding and enhances complement-dependent cytotoxicity. *Front Immunol*. 2017;8:646.
48. Michaelsen TE, et al. The four mouse IgG isotypes differ extensively in bactericidal and opsonophagocytic activity when reacting with the P1.16 epitope on the outer membrane PorA protein of Neisseria meningitidis. *Scand J Immunol*. 2004;59(1):34–39.
49. Collins AM. IgG subclass co-expression brings harmony to the quartet model of murine IgG function. *Immunol Cell Biol*. 2016;94(10):949–954.
50. Klaus GG, et al. Activation of mouse complement by different classes of mouse antibody. *Immunology*. 1979;38(4):687–695.
51. Vattepu R, et al. Sialylation as an important regulator of antibody function. *Front Immunol*. 2022;13:818736.
52. Quast I, et al. Sialylation of IgG Fc domain impairs complement-dependent cytotoxicity. *J Clin Invest*. 2015;125(11):4160–4170.
53. Azeredo da Silveira S, et al. Complement activation selectively potentiates the pathogenicity of the IgG2b and IgG3 isotypes of a high affinity anti-erythrocyte autoantibody. *J Exp Med*. 2002;195(6):665–672.
54. Cobb BA. The history of IgG glycosylation and where we are now. *Glycobiology*. 2020;30(4):202–213.
55. Parekh RB, et al. Association of rheumatoid arthritis and primary osteoarthritis with changes in the glycosylation pattern of total serum IgG. *Nature*. 1985;316(6027):452–457.
56. Ohmi Y, et al. Sialylation converts arthritogenic IgG into inhibitors of collagen-induced arthritis. *Nat Commun*. 2016;7(1):11205.
57. Kaneko Y, et al. Anti-inflammatory activity of immunoglobulin G resulting from Fc sialylation. *Science*. 2006;313(5787):670–673.
58. Murphy CA, et al. Divergent pro- and anti-inflammatory roles for IL-23 and IL-12 in joint autoimmune inflammation. *J Exp Med*. 2003;198(12):1951–1957.
59. Cornelissen F, et al. IL-23 dependent and independent stages of experimental arthritis: no clinical effect of therapeutic IL-23p19 inhibition in collagen-induced arthritis. *PLoS 1*. 2013;8(2):e57553.
60. Dillon SM, et al. Quantifying HIV-1-mediated gut $CD4^+$ T cell deathin the lamina propria aggregate culture (LPAC) model. *Bio Protoc*. 2020;10(2):e3486.
61. Dillon SM, et al. Human intestinal lamina propria $CD1c^+$ dendritic cells display an activated phenotype at steady state and produce IL-23 in response to TLR7/8 stimulation. *J Immunol*. 2010;184(12):6612–6621.
62. Howe R, et al. Evidence for dendritic cell-dependent CD4(+) T helper-1 type responses to commensal bacteria in normal human intestinal lamina propria. *Clin Immunol*. 2009;131(2):317–332.

63. Zhang Q, et al. Fecal metabolomics and potential biomarkers for systemic lupus erythematosus. *Front Immunol*. 2019;10:976.
64. Shen J, et al. Indole-3-acetic acid alters intestinal microbiota and alleviates ankylosing spondylitis in mice. *Front Immunol*. 2022;13:762580.
65. Yang T-H, et al. Supplement of 5-hydroxytryptophan before induction suppresses inflammation and collagen-induced arthritis. *Arthritis Res Ther*. 2015;17(1):364.
66. Rosser EC, et al. Microbiota-derived metabolites suppress arthritis by amplifying aryl-hydrocarbon receptor activation in regulatory B cells. *Cell Metab*. 2020;31(4):837–851.
67. Scott GN, et al. The immunoregulatory enzyme IDO paradoxically drives B cell-mediated autoimmunity. *J Immunol*. 2009;182(12):7509–7517.
68. Criado G, et al. Indoleamine 2,3 dioxygenase-mediated tryptophan catabolism regulates accumulation of Th1/Th17 cells in the joint in collagen-induced arthritis. *Arthritis Rheum*. 2009;60(5):1342–1351.
69. Nakoneczna I, et al. The arthritogenic effect of indole, skatole and other tryptophan metabolites in rabbits. *Am J Pathol*. 1969;57(3):523–538.
70. Brown J, et al. Microbiota-mediated skewing of tryptophan catabolism modulates $CD4^+$ T cells in lupus-prone mice. *iScience*. 2022;25(5):104241.
71. Sonner JK, et al. Dietary tryptophan links encephalogenicity of autoreactive T cells with gut microbial ecology. *Nat Commun*. 2019;10(1):4877.
72. Matsumura M, et al. L-tryptophan 2,3-dioxygenase of a moderate thermophile, Bacillus brevis. Purification, properties and a substrate-mediated stabilization of the quaternary structure. *Biochim Biophys Acta*. 1984;786(1–2):9–17.
73. Zhang X, et al. The oral and gut microbiomes are perturbed in rheumatoid arthritis and partly normalized after treatment. *Nat Med*. 2015;21(8):895–905.
74. Chen J, et al. An expansion of rare lineage intestinal microbes characterizes rheumatoid arthritis. *Genome Med*. 2016;8(1):43.
75. Nishida Y, et al. Pathogenicity of IgG-Fc desialylation and its association with Th17 cells in an animal model of systemic lupus erythematosus [published online June 10, 2023]. *Mod Rheumatol*. https://doi.org/10.1093/mr/road054.
76. Hong H, et al. IL-23 promotes a coordinated B cell germinal center program for class-switch recombination to IgG2b in BXD2 mice. *J Immunol*. 2020;205(2):346–358.
77. Zhang J, et al. Hypoxia and hypoxia-inducible factor signals regulate the development, metabolism, and function of B cells. *Front Immunol*. 2022;13:967576.
78. Gass JN, et al. Activation of an unfolded protein response during differentiation of antibody-secreting B cells. *J Biol Chem*. 2002;277(50):49047–49054.
79. Ma K, et al. IL-17 sustains the plasma cell response via p38-mediated Bcl-xL RNA stability in lupus pathogenesis. *Cell Mol Immunol*. 2021;18(7):1739–1750.
80. Yamada T, et al. B lymphocyte stimulator activates p38 mitogen-activated protein kinase in human Ig class switch recombination. *Am J Respir Cell Mol Biol*. 2005;32(5):388–394.
81. Ercan A, et al. Aberrant IgG galactosylation precedes disease onset, correlates with disease activity, and is prevalent in autoantibodies in rheumatoid arthritis. *Arthritis Rheum*. 2010;62(8):2239–2248.
82. Gracey E, et al. Sexual dimorphism in the Th17 signature of ankylosing spondylitis. *Arthritis Rheumatol*. 2016;68(3):679–689.
83. Kenna TJ, et al. Enrichment of circulating interleukin-17-secreting interleukin-23 receptor-positive γ/Δ T cells in patients with active ankylosing spondylitis. *Arthritis Rheum*. 2012;64(5):1420–1429.
84. Ciccia F, et al. Type 3 innate lymphoid cells producing IL-17 and IL-22 are expanded in the gut, in the peripheral blood, synovial fluid and bone marrow of patients with ankylosing spondylitis. *Ann Rheum Dis*. 2015;74(9):1739–1747.
85. Taams LS. Interleukin-17 in rheumatoid arthritis: trials and tribulations. *J Exp Med*. 2020;217(3):e20192048.
86. Chang H-H, et al. A molecular signature of preclinical rheumatoid arthritis triggered by dysregulated PTPN22. *JCI Insight*. 2016;1(17):e90045.